International Journal of Oral Science www.nature.com/ijos

ARTICLE OPEN

Sclerostin antibody improves alveolar bone quality in the *Hyp* mouse model of X-linked hypophosphatemia (XLH)

Kelsey A. Carpenter[1], Delia O. Alkhatib[1], Bryan A. Dulion[1], Elizabeth Guirado[2], Shreya Patel[1], Yinghua Chen[2], Anne George[2] and Ryan D. Ross[1,3,4]✉

X-linked hypophosphatemia (XLH) is a rare disease of elevated fibroblast growth factor 23 (FGF23) production that leads to hypophosphatemia and impaired mineralization of bone and teeth. The clinical manifestations of XLH include a high prevalence of dental abscesses and periodontal disease, likely driven by poorly formed structures of the dentoalveolar complex, including the alveolar bone, cementum, dentin, and periodontal ligament. Our previous studies have demonstrated that sclerostin antibody (Scl-Ab) treatment improves phosphate homeostasis, and increases long bone mass, strength, and mineralization in the *Hyp* mouse model of XLH. In the current study, we investigated whether Scl-Ab impacts the dentoalveolar structures of *Hyp* mice. Male and female wild-type and *Hyp* littermates were injected with 25 mg·kg^{-1} of vehicle or Scl-Ab twice weekly beginning at 12 weeks of age and euthanized at 20 weeks of age. Scl-Ab increased alveolar bone mass in both male and female mice and alveolar tissue mineral density in the male mice. The positive effects of Scl-Ab were consistent with an increase in the fraction of active (nonphosphorylated) β-catenin, dentin matrix protein 1 (DMP1) and osteopontin stained alveolar osteocytes. Scl-Ab had no effect on the mass and mineralization of dentin, enamel, acellular or cellular cementum. There was a nonsignificant trend toward increased periodontal ligament (PDL) attachment fraction within the Hyp mice. Additional PDL fiber structural parameters were not affected by Scl-Ab. The current study demonstrates that Scl-Ab can improve alveolar bone in adult *Hyp* mice.

International Journal of Oral Science (2023)15:47 ; https://doi.org/10.1038/s41368-023-00252-1

INTRODUCTION

X-linked hypophosphatemia (XLH) is an inherited rickets caused by inactivating mutations in phosphate regulating neutral endopeptidase on the X-chromosome (PHEX). Loss of PHEX results in elevated fibroblast growth factor 23 (FGF23), a circulating phosphaturic hormone that acts on the kidney to decrease phosphate reabsorption and inhibit 1,25-dihydroxyvitamin D production.[1] The resulting hypophosphatemia contributes to poor mineralization of the extracellular matrix in the bone and teeth of XLH patients. Yet, restoration of phosphate homeostasis does not fully rescue impaired mineralization, suggesting that local matrix inhibitors accumulate in the matrix of mineralized tissues.[2] Dentin matrix protein 1 (DMP1) is one such matrix inhibitor that accumulates in the alveolar bone and cellular cementum of the *Hyp* mouse model of XLH.[3] DMP1 regulates FGF23 expression[4] and matrix mineralization independently of PHEX mutations.[5] Osteopontin (OPN) is another established mineralization inhibitor that accumulates in mineralized tissues of patients with XLH[6] and in *Hyp* mice.[3,7] Genetic ablation of OPN improves matrix mineralization without affecting FGF23 expression or correcting hypophosphotamia,[8] in further support of dual systemic and local inhibitory mechanisms driving mineralization defects in XLH.

Between 50%–80% of XLH patients deal with dental complications,[9,10] including abscesses, and periodontal disorders.[10,11] Abnormalities in the matrix of dentoalveolar tissues, including impaired mineralization, large pulp chambers, and interglobular accumulation in dentin[12] likely contribute to recurrent dental abscesses and the high prevalence of periodontitis. A more detailed description of the dentoalveolar tissue pathologies associated with loss of PHEX function has been obtained using *Hyp* mice, which present with the porous alveolar bone, enlarged osteocyte, and cementoctye lacunae, thin acellular cementum, hypomineralized cellular cementum, and detachment of the periodontal ligament (PDL).[3,13] The periodontal defects are associated with impaired mechanical function for the periodontal complex.[3]

Sclerostin is a circulating antagonist to Wnt signaling. Sclerostin null mice have increased bone mass driven by elevated bone formation.[14] In the dentoalveolar compartment, sclerostin null mice have increased alveolar bone mass and acellular and cellular cementum thickness, as well as decreased PDL space.[15] The gene encoding sclerostin (*SOST*) is primarily produced by bone-embedded osteocytes,[16] as well as by cementocytes, particularly during the late stages of cementum development.[17,18] Sclerostin is also expressed by cells within the PDL, both in vivo and in vitro, and its expression is significantly upregulated in response to mechanical loads.[19]

Our previous research found that sclerostin antibody (Scl-Ab) increases long bone mass and mineralization, decreases FGF23

[1]Department of Anatomy & Cell Biology, Rush University Medical Center, Chicago, IL, USA; [2]Department of Oral Biology, The University of Illinois at Chicago, Chicago, IL, USA; [3]Department of Orthopedic Surgery, Rush University Medical Center, Chicago, IL, USA and [4]Department of Microbial Pathogens and Immunity, Rush University Medical Center, Chicago, IL, USA
Correspondence: Ryan D. Ross (Ryan_ross@rush.edu)

Received: 31 March 2023 Revised: 15 September 2023 Accepted: 18 September 2023
Published online: 10 October 2023

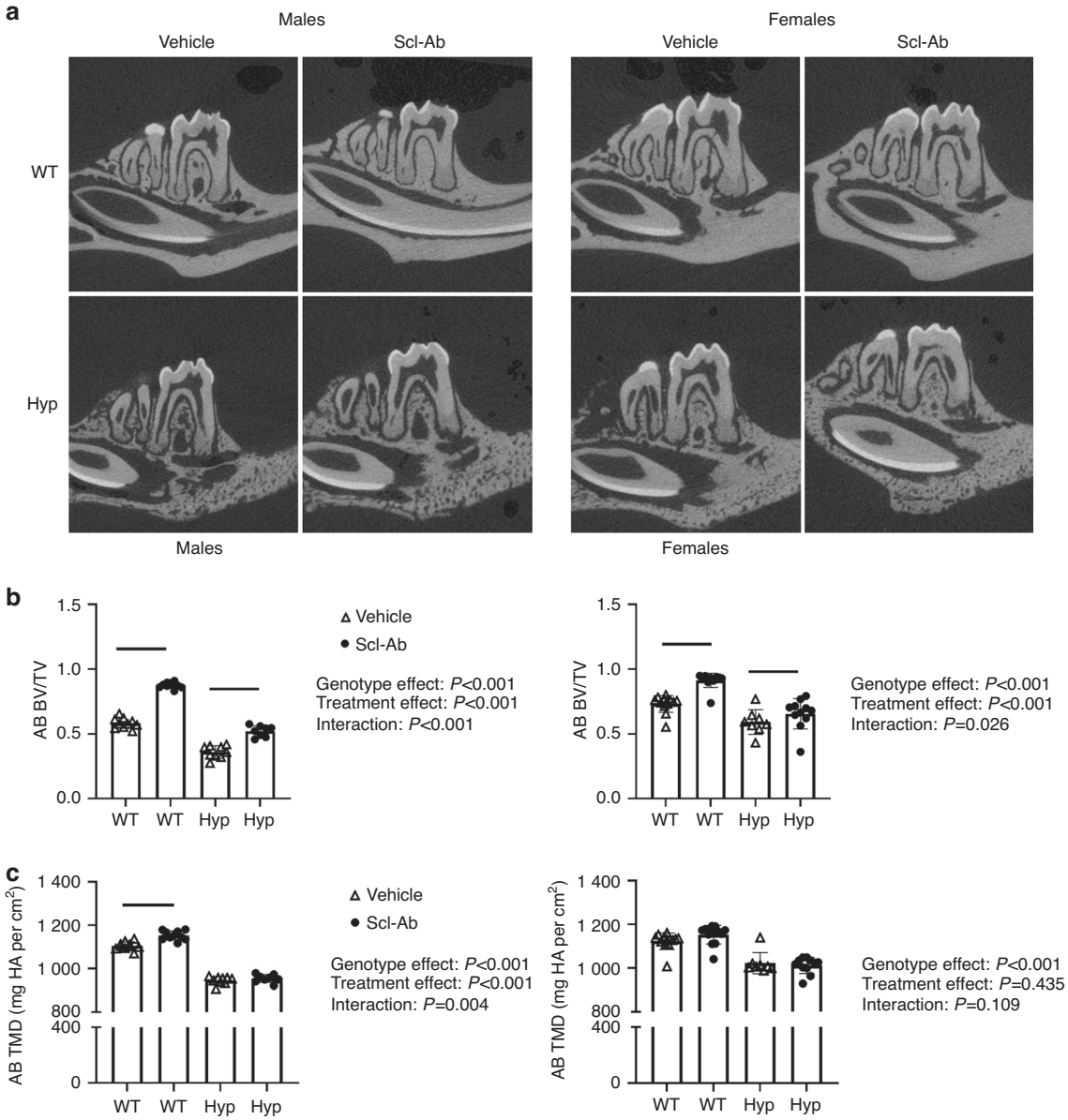

Fig. 1 **a** Representative sagittal microCT images of hemimandibles (top). **b** Alveolar bone volume per total volume and (**c**) tissue mineral density in male (left) and female (right) mice. Data are presented as the mean ± standard deviation. Results from the two-way analysis of variance (ANOVA) are presented in the figure legends. Significant post hoc treatment differences between animals of the same genotype are presented as a horizontal bar. *P* value thresholds are indicated with stars above the bars: *$P < 0.05$; **$P < 0.01$; ***$P < 0.001$; ****$P < 0.000\,1$. The sample sizes ranged between 10 and 14 samples per group

levels, and increases phosphate in growing and adult *Hyp* mice.[20,21] The goal of this study is to evaluate the efficacy of Scl-Ab in improving the dentoalveolar defects in adult *Hyp* mice. We chose to focus on adult mice as dental complications are reported at nearly twice the rate in adult XLH patients when compared to children.[10] We hypothesized that Scl-Ab treated *Hyp* mice will have increased alveolar bone volume, dentin/cementum volume, cellular cementum area, and PDL attachment.

RESULTS

Scl-Ab improves alveolar bone mass in both Hyp and WT mice

Previous characterization of these mice found that Scl-Ab reduces FGF23 levels and increases trabecular bone mass in the distal femoral metaphysis and cortical bone mass in the femoral midshaft.[20]

Hyp mice presented with decreased alveolar bone volume per total volume (AB BV/TV) when compared WT mice in both sexes (Fig. 1 and Supplemental Table 1). Scl-Ab increased AB BV/TV regardless of genotype or sex (Fig. 1). Overall, WT mice exhibited greater increases in AB BV/TV when compared to *Hyp* mice (males: 50% WT, 45% *Hyp*; females: 25% WT, 11% *Hyp*). Increased AB BV/TV following Scl-Ab treatment was primarily due to increased alveolar bone volume (Supplemental Table 1). Scl-Ab increased alveolar bone volume regardless of genotype or sex, although the post hoc comparisons were not significant in the Hyp female mice.

By contrast, increases in alveolar tissue mineral density (AB TMD) in response to Scl-Ab were only observed in male mice. There was also a significant genotype-by-treatment interaction in male mice, attributed to the significant increase in WTs but a lack of a post hoc difference in *Hyp* mice. No significant differences in alveolar tissue mineral density were observed in female mice.

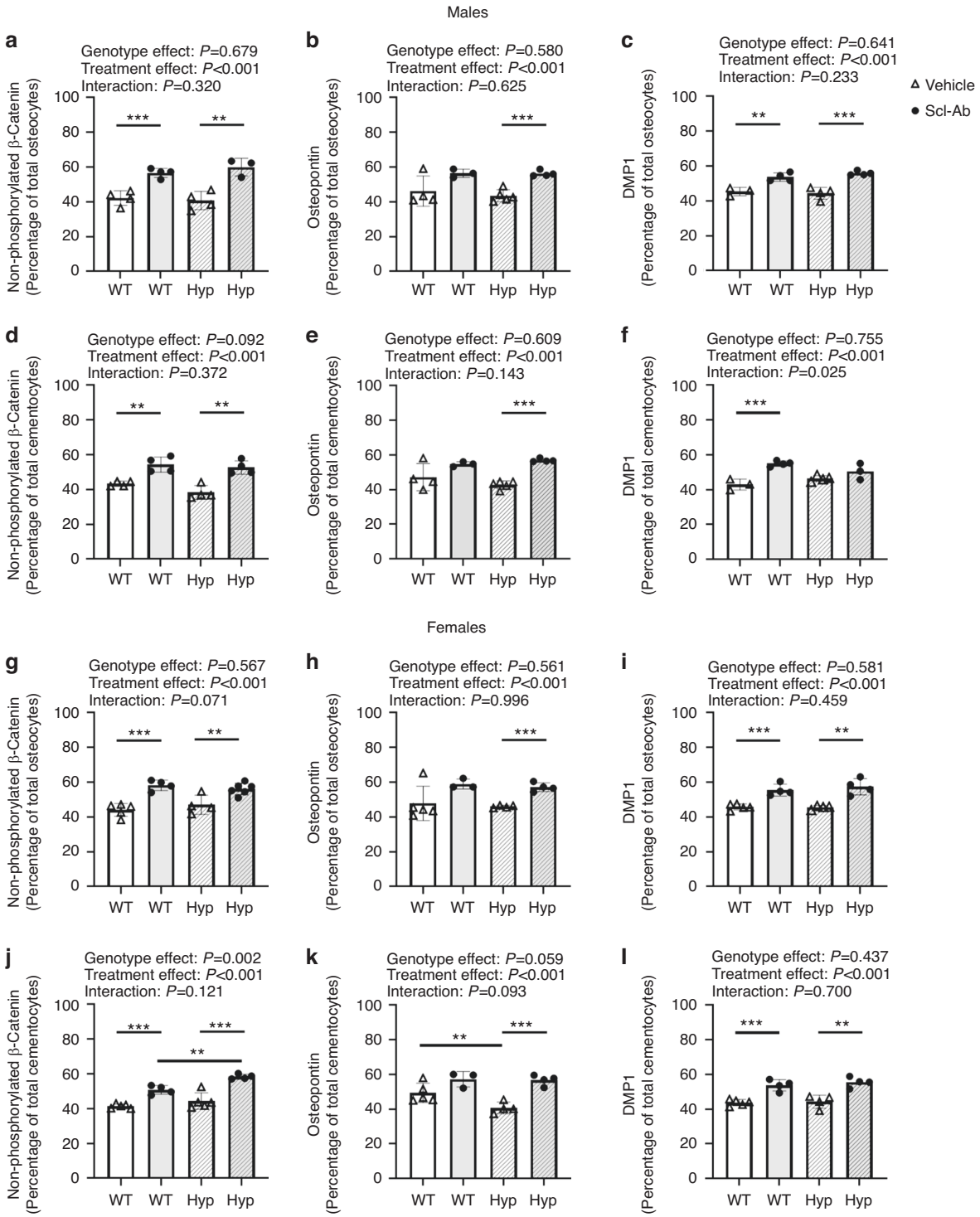

Fig. 2 Quantitative immunostaining of osteocytes in the alveolar bone between the tooth roots of the first molar and cementocytes in the mesial root of the first molar in male (left) and female (right) WT and *Hyp* mice treated with vehicle or Scl-Ab. **a**, **g** Quantitative measurements of the percentage of nonphosphorylated β-catenin-stained osteocytes normalized by the total number of bone-embedded osteocytes within the alveolar bone region of interest. **b, h** Osteopontin stained osteocytes. **c**, **i** DMP1-stained osteocytes. **d**, **j** nonphosphorylated β-catenin-stained cementocytes. **e, k** Osteopontin stained cementocytes (**f**, **l**) DMP1-stained cementocytes. Data are presented as the mean ± standard deviation. Results from the two-way analysis of variance (ANOVA) are presented in the figure legends. Significant post hoc treatment differences between animals of the same genotype are presented as a horizontal bar. *P* value thresholds are indicated with stars above the bars: $^{*}P < 0.05$; $^{**}P < 0.01$; $^{***}P < 0.001$. The sample sizes ranged between 3 and 6 samples per group

Nonphosphorylated (active) β-catenin staining was used to evaluate the activation of Wnt signaling within osteocytes and cementocytes, cells known to express sclerostin.[16–18] The percentage of active β-catenin-stained osteocytes was not affected by genotype (Fig. 2a, g). Scl-Ab treatment increased the percentage of active β-catenin-stained osteocytes in both males and females (treatment effect: $P < 0.001$, both sexes). The percentage of active β-catenin-stained cementocytes was not affected by genotype in

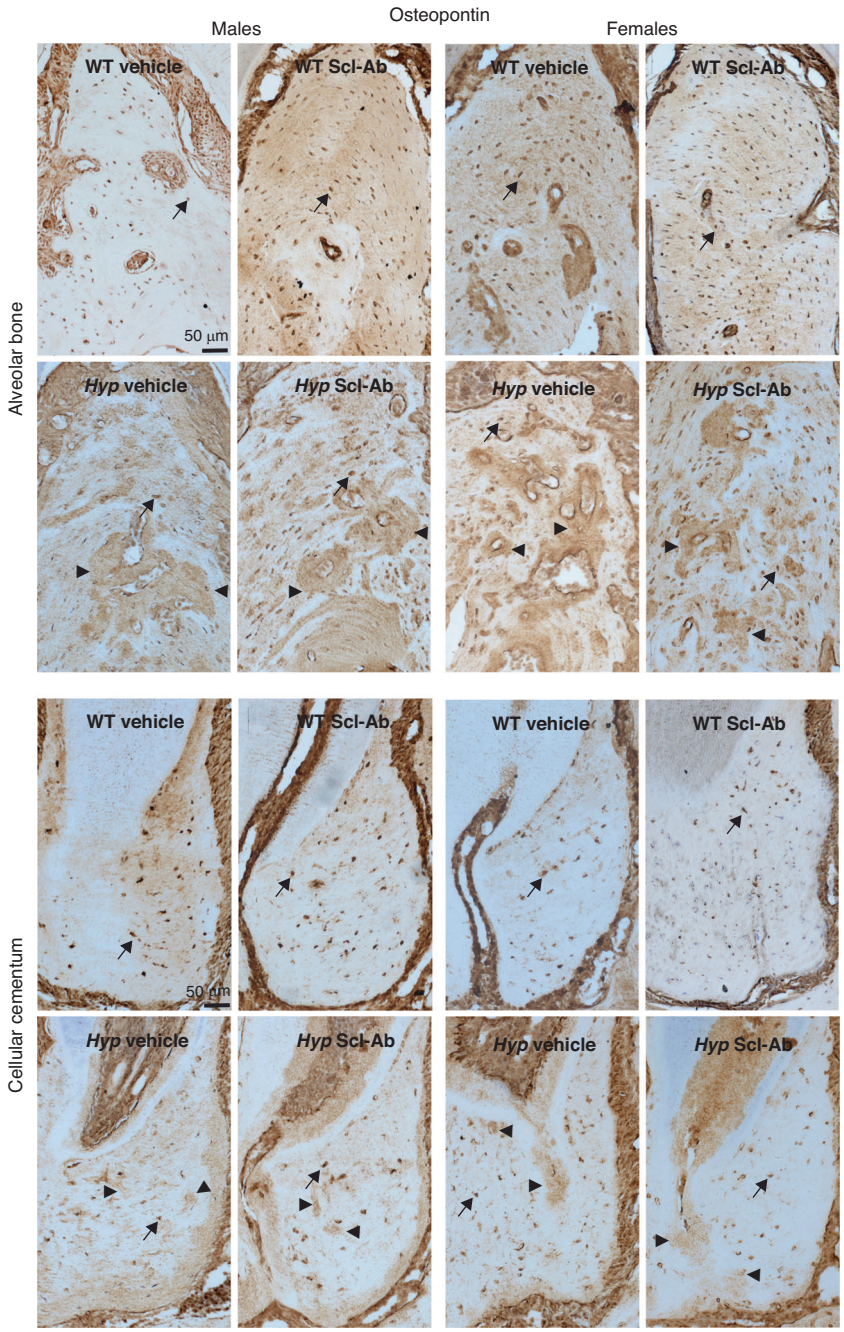

Fig. 3 Osteopontin immunostaining of alveolar bone and cellular cementum in male (left) and female (right) WT and Hyp mice treated with vehicle or Scl-Ab. Alveolar bone was evaluated between the tooth roots of the first molar (M1), while the cellular cementum was evaluated in the mesial root of M1. Arrowheads point to dense regions of OPN staining within the alveolar bone of *Hyp* mice, while arrows indicate positively stained cells

male mice, but there was a significant increase in the percentage of active β-catenin-stained cementocytes in female mice (genotype effect: $P = 0.002$, Fig. 2d, j). Scl-Ab treatment increase the percentage of active β-catenin-stained cementocytes in both male and female mice (treatment effect: $P < 0.001$, Fig. 2d, j). Representative images of active β-catenin-stained alveolar bone and cellular cementum are presented in Supplemental Fig. 1.

Osteopontin (OPN), a critical regulator of matrix mineralization[22] and a protein implicated in the inhibited mineralization of the bones and teeth of XLH patients,[6] was evaluated in both alveolar bone and cellular cementum. At the cellular level, there were no significant differences in the osteocyte (Fig. 2b, h) or cementocyte expression of OPN (Fig. 2h, k). Sclerostin antibody treatment significantly increased OPN expression in both cell types (treatment effect: $P < 0.001$, for all). Within the extracellular matrix, male and female *Hyp* mice present with regions of high OPN staining within the alveolar bone (Fig. 3, black arrows), whereas the WT animals present with lower OPN staining and a more diffuse staining pattern. Scl-Ab did not affect the distribution of OPN of *Hyp* mice of either sex (Fig. 3).

DMP1, a regulator of both matrix mineralization[23] and FGF23 expression,[4] was also evaluated in both alveolar bone and cellular cementum. The percentage of DMP1-stained osteocytes and cementocytes was not affected by genotype in male (Fig. 2c, f) or

Table 1. Cementum and pre-dentin parameters from H&E stained sections

Variable	WT Vehicle	WT Scl-Ab	*Hyp* Vehicle	*Hyp* Scl-Ab	Genotype	Treatment	Interaction
Males							
Acellular Cementum Thickness/μm	5.22 ± 1.78	5.79 ± 1.54	1.94 ± 0.44[b]	1.57 ± 0.45[b]	**<0.001**	0.852	0.369
Pre-Dentin Thickness/μm	4.48 ± 1.04	3.85 ± 2.14	12.37 ± 3.89[b]	11.36 4.68[b]	**<0.001**	0.538	0.887
Cellular Cementum Area/mm^2	0.15 ± 0.08	0.17 ± 0.03	0.15 ± 0.01	0.16 ± 0.04	0.827	0.630	0.933
Females							
Acellular Cementum Thickness/μm	5.91 ± 1.91	5.27 ± 1.66	2.80 ± 1.04[b]	1.72 ± 0.63[b]	**<0.001**	0.147	0.711
Pre-Dentin Thickness/μm	4.34 ± 2.83	4.51 ± 2.98	7.33 ± 1.55	7.14 ± 2.28	**0.018**	0.992	0.870
Cellular Cementum Area/mm^2	0.17 ± 0.08	0.16 ± 0.02	0.13 ± 0.01	0.17 ± 0.08	0.564	0.648	0.281

Sample sizes for each variable are as follows:
Acellular Cementum - $n = 5, 6, 6, 5$ for male WT+vehicle, WT+Scl-Ab, Hyp+vehicle, Hyp+Scl-Ab and $n = 6, 6, 5, 7$ for female WT+vehicle, WT+Scl-Ab, Hyp +vehicle, Hyp+Scl-Ab
Pre-Dentin Thickness - $n = 6, 7, 6, 3$ for male WT+vehicle, WT+Scl-Ab, Hyp+vehicle, Hyp+Scl-Ab and $n = 6, 5. 3, 3$ for female WT+vehicle, WT+Scl-Ab, Hyp +vehicle, Hyp+Scl-Ab
Cellular Cementum Area - $n = 3, 4, 3, 3$ for male WT+vehicle, WT+Scl-Ab, Hyp+vehicle, Hyp+Scl-Ab and $n = 4, 5, 5, 3$ for female WT+vehicle, WT+Scl-Ab, Hyp +vehicle, Hyp+Scl-Ab
[a]Indicates significant differences between vehicle and Scl-Ab-treated mice of the same genotype
[b]Indicates significant differences from vehicle treated WT mice

female mice (Fig. 2i, l). Scl-Ab increased the percentage of DMP1-stained osteocytes and cementocytes in both males and females (treatment effect: $P < 0.001$, both sexes). In male mice, there was a significant interaction effect in the percentage of DMP1-stained cementocytes, as there was a larger increase in WT mice following Scl-Ab treatment than in the Hyp mice (interaction effect: $P = 0.025$). Representative images of DMP1-stained alveolar bone and cellular cementum are presented in Supplemental Fig. 2.

Scl-Ab had limited effects on tooth structures

Male and female *Hyp* mice have significantly decreased enamel volume compared to WT mice (genotype effect: $P = 0.001$, both sexes, Supplemental Table 1). Scl-Ab did not affect the enamel volume in either WT or *Hyp* mice. Enamel tissue mineral density was not affected by either genotype or Scl-Ab treatment. Cementum volume was not affected by either genotype or Scl-Ab treatment. Cementum tissue mineral density was significantly decreased in male *Hyp* mice compared to WT mice, but not in female mice (genotype effect: $P < 0.001$ and 0.698 for males and females, respectively). Scl-Ab treatment significantly reduced the cementum tissue mineral density in male mice but not in female mice (treatment effect: $P = 0.001$ and 0.217 for males and females, respectively).

Male and female *Hyp* mice had significantly decreased dentin volume compared to WT mice (genotype effect: $P < 0.001$, both sexes). Scl-Ab did not affect the dentin volume in either WT or *Hyp* mice. Dentin tissue mineral density was not affected by either genotype or Scl-Ab treatment. Male and female *Hyp* mice have significantly increased pulp volume when compared to WT mice (genotype effect: $P < 0.001$, both sexes). Although there were no Scl-Ab treatment effects in either genotype, there was a significant genotype-treatment interaction in female mice ($P = 0.043$), with Scl-Ab increasing and decreasing pulp volume in WT and *Hyp* mice, respectively.

The acellular cementum layer was significantly thinner in *Hyp* mice of both sexes (genotype effect: $P < 0.001$, both males and females, Table 1, Supplemental Fig. 3). Scl-Ab did not affect the acellular cementum thickness in either WT or *Hyp* mice. The pre-dentin layer was significantly thicker in *Hyp* mice of both sexes (genotype effect: $P < 0.001$ and 0.018, males and females, respectively, Table 1), but there was no treatment effect in either WT or *Hyp* mice (Supplemental Fig. 4). The cellular cementum area was not affected by genotype or treatment (Table 1, Supplemental Fig. 5).

Scl-Ab had limited effects on the PDL

The fraction of tooth root in direct contact with PDL fibers was significantly decreased in *Hyp* mice when compared to WTs (genotype effect: $P < 0.001$, both sexes, Table 2). Scl-Ab did not significantly affect the PDL attachment fraction, likely due to the high variability in *Hyp* samples and the fact that WTs were already at nearly 100% attachment (Table 2 & Fig. 4).

Polarized imaging was used to evaluate PDL fiber angle, length, and width. The quantitation of polarized images using CT-FIRE failed to detect significant genotype or treatment effects in the fiber angle, length or width parameters (Table 2 and Supplemental Fig. 6).

DISCUSSION

Dental complications are common in adults with XLH, with between 50% and 80% of patients reporting oral health complaints.[9,10] Currently, treatment strategies for XLH aim to improve phosphate levels with phosphate and vitamin D supplementation or, more recently, by targeting FGF23 with neutralizing antibodies (Burosumab). While both strategies can improve skeletal pathologies, they appear to differ in their effects on periodontal tissues. Lira Dos Santos et al. compared the effects of vitamin D and FGF23 antibody treatment in *Hyp* mice and noted that while both treatments increased phosphate levels, vitamin D was more effective than FGF23 antibody at improving alveolar bone and acellular cementum thickness.[24] A finding that appears consistent with clinical observations, wherein vitamin D appears to reduce the burden of oral infections.[11] Early data with the FGF23 antibody reported increased dental abscesses following treatment,[25] but more recent data suggests that children treated early with Burosumab have reduced dental abscesses.[26,27] The current study was undertaken to understand whether sclerostin contributes to the dentoalveolar defects and to evaluate the use of sclerostin antibody (Scl-Ab) in adult *Hyp* mice. Our results demonstrate that Scl-Ab can improve alveolar bone in adult *Hyp* mice but does not statistically improve other tissues within the dentoalveolar complex.

The *Hyp* mouse is a well-characterized preclinical model of XLH that features the same elevated FGF23, hypophosphatemia, osteomalacia, and low bone mass noted in XLH.[28] Additionally, *Hyp* mice present with the same decreased mass and mineralization of dentoalveolar tissues.[3,29] More detailed characterization of these tissues has described a multitude of aberrant tissue

Table 2. Periodontal ligament (PDL) parameters from picrosirius red-stained sections

Variable	WT Vehicle	WT Scl-Ab	*Hyp* Vehicle	*Hyp* Scl-Ab	Genotype	Treatment	Interaction
Males							
PDL Attachment Fraction/%	97.78 ± 1.1	97.83 ± 3.1	31.3 ± 11.6[b]	40.06 ± 22.4[b]	**<0.001**	0.487	0.492
PDL Fiber Angle/°	84.0 ± 8.5	90.0 ± 11.4	86.3 ± 14.0	85.3 ± 19.0	0.818	0.636	0.514
PDL Fiber Length/μm	19.1 ± 2.8	21.0 ± 2.1	19.8 ± 4.2	19.3 ± 1.2	0.675	0.541	0.301
PDL Fiber Width/μm	2.1 ± 0.1	2.1 ± 0.2	2.2 ± 0.1	2.1 ± 0.1	0.817	0.908	0.400
Females							
Periodontal Ligament Attachment Fraction/%	96.58 ± 4.8	96.86 ± 2.1	53.53 ± 32.6[b]	70.56 ± 16.2[b]	**<0.001**	0.243	0.258
PDL Fiber Angle/°	85.1 ± 31.9	75.0 ± 29.4	104.5 ± 21.1	89.0 ± 28.4	0.148	0.264	0.058
PDL Fiber Length/μm	22.1 ± 3.2	21.2 ± 2.5	21.3 ± 2.6	19.8 ± 2.8	0.325	0.269	0.067
PDL Fiber Width/μm	2.1 ± 0.1	2.1 ± 0.1	2.2 ± 0.2	2.2 ± 0.1	0.125	0.698	0.608

Sample sizes are as follows:
$n = 4, 4, 5, 4$ for male WT+vehicle, WT+Scl-Ab, Hyp+vehicle, Hyp+Scl-Ab and $n = 7, 5, 4, 5$ for female WT+vehicle, WT+Scl-Ab, Hyp+vehicle, Hyp+Scl-Ab
[a]Indicates significant differences between vehicle and Scl-Ab-treated mice of the same genotype
[b]Indicates significant differences from vehicle treated WT mice

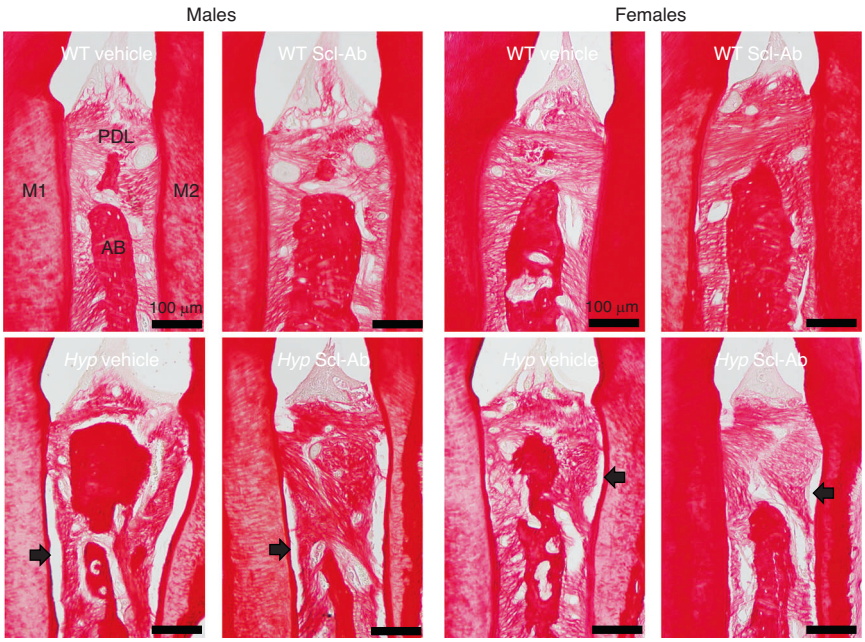

Fig. 4 Picrosirius red staining of the periodontal ligament (PDL) in male (left) and female (right) WT and *Hyp* animals treated with vehicle or Scl-Ab ligament. The root surfaces of the first (M1) and second molar (M2), as well as the alveolar bone (AD), are marked. Arrows point to regions of detachment between the PDL and the tooth roots. The sample sizes ranged between 4 to 7 per group and are presented in Table 2

structures, including porous alveolar bone, enlarged osteocyte, and cementoctye lacunae, thin acellular cementum, hypomineralized cellular cementum, and detachment of the periodontal ligament (PDL).[3,13] The defects noted in the alveolar bone, cementum, and periodontal ligament likely contribute to an increase risk of excessive tooth mobility and subsequent loss.[11] Bacterial invasion and the eventual development of dental abscesses is likely due to the poorly mineralized dentin and enamel structures and subsequent cracking that can allow bacteria to reach the pulp chamber.[30,31] Finally, poor alveolar bone quality likely contributes to the high rates of implant failures reported in XLH patients.[10]

The clinical implications of the current study remain to be determined. Due to the lack of a Scl-Ab effect on the dentin, enamel, or dental pulp, it is unclear whether Scl-Ab would reduce the prevalence of dental abscesses in XLH patients. However, clinical reports have noted general alveolar bone loss as a contributing factor to tooth mobility in Hyp mice[3] and tooth loss in XLH patients.[11,32] Therefore, improving alveolar bone quality and the effects on the PDL, even if nonsignificant, may improve tooth retention for XLH patients. Additionally, as alveolar bone quality contributes to reduced dental implant success, the positive effects of Scl-Ab on alveolar bone quality may improve implant fixation. Although Scl-Ab has not been tested in Hyp mice with implants, it can increase implant fixation within the long bones of severely osteoporotic rodents.[33] However, future work evaluating tooth mobility, tooth abscess development, or the stability of dental implants following Scl-Ab treatment is needed. One limitation worth noting is that our alveolar bone measurements were made between the tooth roots, or the bone within the furcation. Although this likely reflects general alveolar bone response, cervically located alveolar bone is a critical component of tooth stability and is not reflected in our alveolar bone measurements.

Our previous publications have demonstrated the positive effects of Scl-Ab treatment on FGF23 and phosphate levels, as well as long bone mass, mineralization and strength in *Hyp* mice.[20,21] The current study expands these findings to show that Scl-Ab has positive effects on alveolar bone in *Hyp* mice, perhaps unsurprisingly, as osteocytes within the alveolar bone are known to express sclerostin protein.[16,18] Alveolar osteocytes show increased expression of nuclear β-catenin, indicating the activation of Wnt signaling, as well as increased expression of osteopontin and DMP1, two genes associated with osteocytic differentiation that have been previously reported to be responsive to Wnt signaling.[34,35] Interestingly, cementocytes within the cellular cementum and cells within the PDL also express sclerostin[17–19] and in the current study, cementocytes also show increased Wnt signaling with Scl-Ab treatment. Further, unlike enamel and dentin, which do not generally undergo remodeling, cellular cementum, and the PDL are able to remodel and repair, much like the alveolar bone tissue,[12] yet Scl-Ab had little to no effect on either the cellular cementum or the PDL. It is unclear why the non-bone tissues are not as responsive to Scl-Ab treatment. It is possible that the relatively late stage of development evaluated in this study—near the end of skeletal maturity and past molar eruption—contributed to the limited effects outside of bone. We designed the experiment to test the effects of Scl-Ab in adult mice, as dental complications are a common complaint in adult XLH patients.[10] However, it is worth noting that clinical data have suggested that early and sustained treatment starting in childhood had the most significant impact on preventing periodontitis in XLH patients.[11] Indeed, new data reported that children with XLH that receive Burosumab before they reach 5 years of age had fewer dental abscesses than children treated with conventional phosphate supplementation, but children treated after 5 years of age did not see the same benefit.[27] Therefore, future work should aim to evaluate whether early Scl-Ab treatment would have a more significant benefit on periodontal diseases. Although it is worth noting that activation of Wnt signaling has a complex spatiotemporal expression pattern during tooth development[36] and constitutive activation can delay tooth eruption,[37–39] so care must be taken to identify the appropriate age for intervention.

Similar positive effects of Scl-Ab on alveolar bone were observed in the DMP1 null mouse model of autosomal recessive hypophosphatemic rickets (ARHR).[40] However, unlike the current study, the authors report that Scl-Ab improved the cellular cementum and PDL organization, although it is worth noting that these effects were not compared quantitatively, as in the current study. Interestingly, Scl-Ab had no effect on circulating FGF23 in the ARHR mouse,[40] unlike in the *Hyp* mouse, where we previously reported decreased FGF23 following Scl-Ab treatment.[20,21] The positive effects in the alveolar bone of both the ARHR and *Hyp* mouse models suggest that these are likely a direct effect of sclerostin suppression, rather than a secondary effect of improved phosphate metabolism. However, directly assessing the relative contributions of tissue level and systemic changes is difficult. Indeed, although data from the sclerostin knockout mouse has demonstrated increased alveolar bone mass and increased cementum thickness,[15] systemic characterization of mineral metabolism in this mouse has found reduced FGF23 and increased vitamin D when compared to WT littermates.[41] Therefore, we cannot rule out that the Scl-Ab mediated suppression of circulating FGF23 also contributes to improve matrix mineralization.

Despite increased alveolar bone material density via microCT, the diffuse accumulation of OPN failed to improve with the Scl-Ab effect. Abnormal OPN accumulation, in the form of dense staining around osteocytic lacunae, has previously been described in the alveolar bone, dentin, calvaria, and tibia of *Hyp* mice and XLH patients[6,24] and likely contributes to impair mineralization of XLH tissues. Indeed, genetically ablating OPN in *Hyp* mice reduced unmineralized osteoid accumulation in long bones.[8] While the alveolar bone material density would suggest a reduction in osteoid, a limitation of this study is that we did not have sections of undecalcified samples to directly measure osteoid area. Our previous studies found a minor decrease in osteoid following Scl-Ab treatment in the long bones of *Hyp* mice,[20,21] but it is unclear whether this same effect occurs in alveolar bone, and while the lack of tissue mineral density effects suggest that mineralization is not affected by Scl-Ab treatment, the resolution of microCT scanning may not be sufficient to detect subtle changes in osteoid thickness.

Although direct sex comparisons were not part of our study design, we evaluated both male and female *Hyp* mice. Scl-Ab positively affected alveolar bone mass in both, but the magnitude change appears to be greater in males, while statistically significant changes in alveolar bone TMD were only present in males. It is unclear whether these differences are due to the X-linked nature of the disease or sex-specific responses to Scl-Ab. XLH is an autosomal dominant disease and therefore, affects both males and females.[42] Clinically, there does not appear to be biochemical differences between male and female XLH patients.[43] However, there have been reports that height reduction is more significant in males.[44] Interestingly, endodontic infections are noted to be more common in males with XLH, while periodontal defects are not different between males and females.[45] Clinically, Scl-Ab is approved for the treatment of postmenopausal women and few studies have been performed in men. One clinical safety study that did include both found that both had increased bone mass but did not directly compare between sexes.[46] A direct sex comparison of Scl-Ab treatment was performed in a mouse model of osteogenesis imperfecta and reported that some skeletal changes were greater in male mice,[47] consistent with the current study. Therefore, it seems likely that sclerostin suppression may affect males more than females, but the cause for these sex-specific responses is unknown.

In summary, our study indicates that Scl-Ab can increase alveolar bone mass and mineralization in the *Hyp* mouse model of XLH. While improving alveolar bone quality is likely to have positive effects on the oral health of XLH patients, whether Scl-Ab represents a viable clinical treatment option for XLH patients warrants further study.

MATERIALS AND METHODS

Animals

Female heterozygous (+/*Hyp*, strain 000528) and male wild-type (WT; +/y) mice were purchased from Jackson Laboratory (Bar Harbor, ME, USA). The breeding strategy generated heterozygous (+/*Hyp*) and WT females and hemizygous (*Hyp*/y) and WT males. Mice were weaned at 4 weeks, caged in groups of 3 to 5, maintained on a 12-hour dark/light cycle, and provided standard chow (2018, Teklad) and water ad libitum. All mice were randomly assigned twice weekly 25 mg/kg subcutaneous injections of either Scl-Ab (Amgen Inc, Thousand Oaks, CA and UCB, Brussels, Belgium) or vehicle (saline). The dose was chosen based on previous rodent studies.[48] Importantly, anabolic responses have been noted in doses as low as 5 mg·kg^{-1}.[49] Injections began at 12 weeks of age and continued for 8 weeks, until sacrifice at 20 weeks of age.

Tissues were collected 24-hours after the last injection. Blood was collected via cardiac puncture and allowed to clot at room temperature for 30 mins before centrifugation at 3 400 r·min^{-1} for 15 min at 4 °C for serum separation. Mandibles were collected in 10% formalin and after 48 h were separated into left and right hemi-mandibles and stored in 70% ethanol. The total sample size for each group was 12, 12, 10, and 10 for male WT vehicle treated, WT Scl-Ab treated, *Hyp* vehicle treated, and *Hyp* Scl-Ab treated,

respectively, and 13, 14, 10, and 12 for female WT vehicle treated, WT Scl-Ab treated, Hyp vehicle treated, and Hyp Scl-Ab treated, respectively. The sample size used was based on our tissues available from our published study.[20] All animal studies were approved by the Rush University Institutional Animal Care and Use Committee and were designed to confirm to ARRIVE guidelines. No unexpected adverse events were encountered.

Micro-computed tomography

Left hemi-mandibles were micro-computed tomography (microCT, μCT50, Scanco Medical). Four separate analyses were performed to characterize alveolar bone, enamel, dentin/cementum complex, and pulp volume. Left hemi-mandibles were microCT scanned while submerged in distilled water. Hemimandibles were placed into a custom designed sample holder with the buccal plane facing downwards, and images were collected in the sagittal plane. Scanning parameters were 55 kVp and 145 μA, with a 500 ms integration time, a 6 μm isotropic voxel size, and a 0.5 mm aluminum filter. Alveolar bone was evaluated on the furcation area between the roots of the first molar, as described elsewhere.[50] A total number of 70 slices were evaluated within the middle of the first molar. The primary outcome of alveolar bone was bone volume per total volume (BV/TV). Enamel and dental pulp regions of interest were identified in the first molar using previously defined thresholding techniques.[51] Enamel was analyzed with a lower threshold of 1 600 mg HA per cm^3, an upper threshold of 3000 mg HA/cm^3, and Gaussian filter settings of 0.8 and 1. Dental pulp was analyzed with a lower threshold of 500 mg HA per cm^3, an upper threshold of 650 mg HA per cm^3, and Gaussian filter settings of 0.8 and 1. Cementum was analyzed with a lower threshold of 650 mg HA per cm^3, an upper threshold of 985 mg HA per cm^3, and Gaussian filter settings of 2 and 4. Dentin was analyzed with a lower threshold of 985 mg HA per cm^3, an upper threshold of 1 600 mg HA per cm^3, and Gaussian filter settings of 2 and 4.

Hematoxylin and Eosin Staining

Right and left hemi-mandibles were washed with deionized water, decalcified in 14% ethylenediaminetetraacetic acid disodium salt dihydrate (pH 7.4) (EDTA, Fisher Scientific) for 5 weeks and dehydrated and embedded in Ribbon Pro paraffin (Thermo Scientific). Sections (5 μm thick) were cut either in the coronal or sagittal planes depending on the analysis, using a Leica RM2255. Sections were stained with hematoxylin and eosin (H&E) to evaluate pre-dentin and acellular cementum thicknesses on the distal root of the first molar from sagittal sections (Nikon Eclipse 80i with Osteomeasure). Cellular cementum area was evaluated on the mesial root of the first molar from coronal sections, as reported by others.[3,24]

Picrosirius Red Staining, Polarized Imaging and CT-FIRE Analysis

Hemi-mandible sections were stained using 0.2% phosphomolybdic acid (Electron Microscopy Sciences). Phosphomolybdic acid was added for 3 min and the slides were subsequently rinsed with water. Sirius Red, 0.1% in saturated picric acid was added to the slides for 90 min, followed by two washes in 0.01 N hydrochloric acid, dehydration, and mounting with Permount (Fisher Chemical Permount Mounting Medium).

Stained sagittal sections were imaged under brightfield light (Nikon Eclipse 80i with Osteomeasure) to quantitate the PDL attachment fraction. The PDL attachment fraction was defined as the total length of acellular cementum along the distal root of the first molar in contact with the PDL, which was subsequently normalized to the total length of the acellular cementum. Slides were also imaged under polarized light to visualize collagen fiber orientation (Carl Zeiss AG Axio Observer D1 Inverted Microscope). Polarized images were then evaluated for PDL fiber length, width and angle using CT-FIRE Matlab extension.[52]

Immunohistochemistry

Sample sections were de-paraffinized and rehydrated. Antigen retrieval was performed by incubating samples in trypsin or sodium citrate (Sigma) at 37 °C for 30–45 min. The slides were washed with tris-buffered saline three times followed by blocking in 3% H_2O_2 for 10 min at room temperature. Samples were incubated at 4 °C overnight in primary antibody for OPN (Invitrogen) at a 1:500 dilution, nonphosphorylated Beta-catenin (Cell Signaling) at a 1:100 dilution, or DMP1 (synthesized in-house, see[53]) at a 1:100 dilution. Anti-Rabbit biotinylated secondary antibody was applied to the samples at a 1:300 dilution for 30 min at room temperature. A tyramide signal amplification kit (Perkin Elmer) was used to amplify the binding signal followed by a DAB Peroxidase Substrate Kit (Vector). Immunohistochemistry staining in the alveolar bone was visualized between the mesial and distal roots of the first molar on coronal sections.

The number of osteocytes within the alveolar bone positively stained with nonphosphorylated β-catenin, osteopontin, or DMP1 was quantified by counting the number of positively stained osteocytes and the total number of osteocytes within the alveolar bone (Osteomeasure, OsteoMetrics). A similar approach was used to quantify the number of positively stained cementocytes in the cellular cementum of the mesial root of M1. All cells were counted at 20x magnification using 5–6 separate images to span the entirety of the alveolar bone between the mesial and distal roots of the first and 4–5 separate images to span the entirety of the mesial root cellular cementum surface. The percentage of positively stained osteocytes and cementocytes was calculated by dividing the number of positively stained cells by the total number of stained and unstained cells and multiplying by 100%. The individual sample sizes for each outcome ranged between 3 and 6 per group.

Statistical analysis

Quantitative variables were compared separately for males and females using a two-way analysis of variance (ANOVA) with genotype and treatment as the independent factors. When main effects were significant, post hoc analysis (independent student's T-test) was performed to compare the effects of the Scl-Ab treatment. A P value of <0.05 was considered statistically significant.

DATA AVAILABILITY

All data associated with this study are presented in the paper.

ACKNOWLEDGEMENTS

Sclerostin antibody was provided by Amgen Inc, Thousand Oaks, CA, USA, and UCB, Brussels, Belgium. The authors would like to thank Reid Davison, Chris Mestyanek, and Ashley Edmond for their contributions to this manuscript. Funding: Research reported in this publication was supported by the National Institute of Arthritis and Musculoskeletal and Skin Diseases and the National Institute of Dental and Craniofacial Research of the National Institute of Health under award numbers K01AR073923 and R03DE029873, respectively. The content is solely the responsibility of the authors and does not necessarily represent the official views of the National Institutes of Health.

AUTHOR CONTRIBUTIONS

K.A. Carpenter contributed to the conception, design, acquisition, analysis, and interpretation, drafted and critically revised the manuscript. E. Guirado and Y. Chen contributed to the design, acquisition, analysis, and interpretation, and drafted and critically revised the manuscript. B.A. Dulion, D.O. Alkhatib, and S. Patel contributed to that data acquisition and critically revised the manuscript. A. George and R.D. Ross contributed to the conception, design, acquisition, analysis, and interpretation, drafted and critically revised the manuscript. All authors gave final approval and agree to be accountable for all aspects of the work.

ADDITIONAL INFORMATION

Supplementary information The online version contains supplementary material available at https://doi.org/10.1038/s41368-023-00252-1.

Competing interests: The authors declared no potential conflicts of interest with respect to the research and/or publication of this article.

REFERENCES

1. Carpenter, T. O., Imel, E. A., Holm, I. A., Jan de Beur, S. M. & Insogna, K. L. A clinician's guide to X-linked hypophosphatemia. *J. Bone Min. Res* **26**, 1381–1388 (2011).
2. Liu, S., Tang, W., Zhou, J., Vierthaler, L. & Quarles, L. D. Distinct roles for intrinsic osteocyte abnormalities and systemic factors in regulation of FGF23 and bone mineralization in Hyp mice. *Am. J. Physiol. Endocrinol. Metab.* **293**, E1636–E1644 (2007).
3. Zhang, H. et al. Dentoalveolar Defects in the Hyp Mouse Model of X-linked Hypophosphatemia. *J. Dent. Res* **99**, 419–428 (2020).
4. Martin, A. et al. Bone proteins PHEX and DMP1 regulate fibroblastic growth factor Fgf23 expression in osteocytes through a common pathway involving FGF receptor (FGFR) signaling. *FASEB J.* **25**, 2551–2562 (2011).
5. Martin, A. et al. Overexpression of the DMP1 C-terminal fragment stimulates FGF23 and exacerbates the hypophosphatemic rickets phenotype in Hyp mice. *Mol. Endocrinol.* **26**, 1883–1895 (2012).
6. Boukpessi, T. et al. Osteopontin and the dento-osseous pathobiology of X-linked hypophosphatemia. *Bone* **95**, 151–161 (2017).
7. Barros, N. M. et al. Proteolytic processing of osteopontin by PHEX and accumulation of osteopontin fragments in Hyp mouse bone, the murine model of X-linked hypophosphatemia. *J. Bone Min. Res* **28**, 688–699 (2013).
8. Hoac, B. et al. Genetic Ablation of Osteopontin in Osteomalacic Hyp Mice Partially Rescues the Deficient Mineralization Without Correcting Hypophosphatemia. *J. Bone Miner. Res.* **35**, 2032–2048 (2020).
9. Hanisch, M., Bohner, L., Sabandal, M. M. I., Kleinheinz, J. & Jung, S. Oral symptoms and oral health-related quality of life of individuals with x-linked hypophosphatemia. *Head. Face Med.* **15**, 8 (2019).
10. Skrinar, A. et al. The Lifelong Impact of X-Linked Hypophosphatemia: Results From a Burden of Disease Survey. *J. Endocr. Soc.* **3**, 1321–1334 (2019).
11. Biosse Duplan, M. et al. Phosphate and Vitamin D Prevent Periodontitis in X-Linked Hypophosphatemia. *J. Dent. Res* **96**, 388–395 (2017).
12. Foster, B. L., Nociti, F. H. Jr & Somerman, M. J. The rachitic tooth. *Endocr. Rev.* **35**, 1–34 (2014).
13. Fong, H. et al. Aberrant cementum phenotype associated with the hypophosphatemic hyp mouse. *J. Periodontol.* **80**, 1348–1354 (2009).
14. Li, X. et al. Targeted deletion of the sclerostin gene in mice results in increased bone formation and bone strength. *J. Bone Miner. Res.* **23**, 860–869 (2008).
15. Kuchler, U. et al. Dental and periodontal phenotype in sclerostin knockout mice. *Int J. Oral. Sci.* **6**, 70–76 (2014).
16. van Bezooijen, R. L. et al. Sclerostin is an osteocyte-expressed negative regulator of bone formation, but not a classical BMP antagonist. *J. Exp. Med.* **199**, 805–814 (2004).
17. Lehnen, S. D., Götz, W., Baxmann, M. & Jäger, A. Immunohistochemical evidence for sclerostin during cementogenesis in mice. *Ann. Anat.* **194**, 415–421 (2012).
18. Jager, A., Gotz, W., Lossdorfer, S. & Rath-Deschner, B. Localization of SOST/sclerostin in cementocytes in vivo and in mineralizing periodontal ligament cells in vitro. *J. Periodontal. Res* **45**, 246–254 (2010).
19. Nam, Y. S. et al. Sclerostin in periodontal ligament: Homeostatic regulator in biophysical force-induced tooth movement. *J. Clin. Periodontol.* **49**, 932–944 (2022).
20. Carpenter, K. A. et al. Sclerostin antibody improves phosphate metabolism hormones, bone formation rates, and bone mass in adult Hyp mice. *Bone* **154**, 116201 (2021).
21. Carpenter, K. A. & Ross, R. D. Sclerostin Antibody Treatment Increases Bone Mass and Normalizes Circulating Phosphate Levels in Growing Hyp Mice. *J. Bone Min. Res* **35**, 596–607 (2020).
22. McKee, M. D. & Nanci, A. Osteopontin: an interfacial extracellular matrix protein in mineralized tissues. *Connect Tissue Res* **35**, 197–205 (1996).
23. George, A., Guirado, E. & Chen, Y. in *Biomineralization*. (eds K Endo, T Kogure & H Nagasawa) 137–145 (Springer Singapore).
24. Lira dos Santos, E. J. et al. Effects of Active Vitamin D or FGF23 Antibody on Hyp Mice Dentoalveolar Tissues. *J. Dent. Res.* **100**, 1482–1491 (2021).
25. Imel, E. A. et al. Burosumab versus conventional therapy in children with X-linked hypophosphataemia: a randomised, active-controlled, open-label, phase 3 trial. *Lancet* **393**, 2416–2427 (2019).
26. Gadion, M. et al. Burosumab and Dental Abscesses in Children With X-Linked Hypophosphatemia. *JBMR* **6**, e10672 (2022).
27. Ward, L. M. et al. Effect of Burosumab Compared With Conventional Therapy on Younger vs Older Children With X-linked Hypophosphatemia. *J. Clin. Endocrinol. Metab.* **107**, e3241–e3253 (2022).
28. Eicher, E. M., Southard, J. L., Scriver, C. R. & Glorieux, F. H. Hypophosphatemia: mouse model for human familial hypophosphatemic (vitamin D-resistant) rickets. *Proc. Natl Acad. Sci. USA* **73**, 4667–4671 (1976).
29. Coyac, B. R. et al. Tissue-specific mineralization defects in the periodontium of the Hyp mouse model of X-linked hypophosphatemia. *Bone* **103**, 334–346 (2017).
30. Chaussain-Miller, C. et al. Dentin structure in familial hypophosphatemic rickets: benefits of vitamin D and phosphate treatment. *Oral. Dis.* **13**, 482–489 (2007).
31. Goodman, J. R., Gelbier, M. J., Bennett, J. H. & Winter, G. B. Dental problems associated with hypophosphataemic vitamin D resistant rickets. *Int J. Paediatr. Dent.* **8**, 19–28 (1998).
32. Ye, L., Liu, R., White, N., Alon, U. S. & Cobb, C. M. Periodontal status of patients with hypophosphatemic rickets: a case series. *J. Periodontol.* **82**, 1530–1535 (2011).
33. Virdi, A. S. et al. Sclerostin antibody treatment improves implant fixation in a model of severe osteoporosis. *J. Bone Jt. Surg. Am.* **97**, 133–140 (2015).
34. El-Tanani, M., Platt-Higgins, A., Rudland, P. S. & Campbell, F. C. Ets gene PEA3 cooperates with beta-catenin-Lef-1 and c-Jun in regulation of osteopontin transcription. *J. Biol. Chem.* **279**, 20794–20806 (2004).
35. Friedman, M. S., Oyserman, S. M. & Hankenson, K. D. Wnt11 promotes osteoblast maturation and mineralization through R-spondin 2. *J. Biol. Chem.* **284**, 14117–14125 (2009).
36. Tokavanich, N., Wein, M. N., English, J. D., Ono, N. & Ono, W. The Role of Wnt Signaling in Postnatal Tooth Root Development. *Front. Dent. Med.* **2**, 769134 (2021)
37. Jarvinen, E., Shimomura-Kuroki, J., Balic, A., Jussila, M. & Thesleff, I. Mesenchymal Wnt/beta-catenin signaling limits tooth number. *Development* **145**, (2018)
38. Kim, T. H. et al. Col1a1-cre mediated activation of β-catenin leads to aberrant dento-alveolar complex formation. *Anat. Cell Biol.* **45**, 193–202 (2012).
39. Kim, T. H. et al. Constitutive stabilization of ß-catenin in the dental mesenchyme leads to excessive dentin and cementum formation. *Biochem Biophys. Res Commun.* **412**, 549–555 (2011).
40. Ren, Y. et al. Sclerostin antibody (Scl-Ab) improves osteomalacia phenotype in dentin matrix protein 1(Dmp1) knockout mice with little impact on serum levels of phosphorus and FGF23. *Matrix Biol.* **52-54**, 151–161 (2016).
41. Ryan, Z. C. et al. Sclerostin alters serum vitamin D metabolite and fibroblast growth factor 23 concentrations and the urinary excretion of calcium. *Proc. Natl Acad. Sci. USA* **110**, 6199–6204 (2013).
42. Hawley, S. et al. Prevalence and Mortality of Individuals With X-Linked Hypophosphatemia: A United Kingdom Real-World Data Analysis. *J. Clin. Endocrinol. Metab.* **105**, e871–e878 (2020).
43. Laurent, M. R. et al. Consensus Recommendations for the Diagnosis and Management of X-Linked Hypophosphatemia in Belgium. *Front. Endocrinol.* **12**, 641543 (2021).
44. Rafaelsen, S., Johansson, S., Ræder, H. & Bjerknes, R. Hereditary hypophosphatemia in Norway: a retrospective population-based study of genotypes, phenotypes, and treatment complications. *Eur. J. Endocrinol.* **174**, 125–136 (2016).
45. Larsson, A. et al. Dental health of patients with X-linked hypophosphatemia: A controlled study. *Front Oral. Health* **4**, 1087761 (2023).
46. Padhi, D. et al. Multiple doses of sclerostin antibody romosozumab in healthy men and postmenopausal women with low bone mass: A randomized, double-blind, placebo-controlled study. *J Clin Pharmacol*, (2013).
47. Cardinal, M. et al. Gender-Related Impact of Sclerostin Antibody on Bone in the Osteogenesis Imperfecta Mouse. *Front Genet* **12**, 705505 (2021).
48. Kim, S. W. et al. Sclerostin antibody administration converts bone lining cells into active osteoblasts. *J. Bone Miner. Res.* **32**, 892–901 (2017).
49. Chouinard, L. et al. Carcinogenicity risk assessment of romosozumab: A review of scientific weight-of-evidence and findings in a rat lifetime pharmacology study. *Regul. Toxicol. Pharm.* **81**, 212–222 (2016).
50. Chen, Y., Zhang, Y., Ramachandran, A. & George, A. DSPP Is Essential for Normal Development of the Dental-Craniofacial Complex. *J. Dent. Res* **95**, 302–310 (2016).
51. Chavez, M. B. et al. Guidelines for Micro–Computed Tomography Analysis of Rodent Dentoalveolar Tissues. *JBMR* **5**, e10474 (2021).
52. Bredfeldt, J. S. et al. Computational segmentation of collagen fibers from second-harmonic generation images of breast cancer. *J. Biomed. Opt.* **19**, 16007 (2014).
53. Srinivasan, R., Chen, B., Gorski, J. P. & George, A. Recombinant expression and characterization of dentin matrix protein 1. *Connect. Tissue Res.* **40**, 251–258 (1999).